Differential medial temporal lobe and default-mode network functional connectivity and morphometric changes in Alzheimer's disease

Kamil A. Grajski[1] and Steven L. Bressler[2], for the Alzheimer's disease Neuroimaging Initiative[3]

Correspondence to: Dr. Kamil A. Grajski,
NuroSci, LLC.,
525 South Flagler Drive,
Suite 21CD, West Palm Beach,
FL, 33401,
USA
E-mail: kgrajski@nurosci.com

Abstract

We report group level differential detection of functional connectivity disruption and morphometric changes in the CN to MCI transition in an age-, education- and gender-matched 105 subjects ADNI database, using same-session structural MRI and rsfMRI. In Dementia-MCI and Dementia-CN comparisons, but not MCI-CN comparisons of FreeSurfer estimates of thickness in 68 cortical regions, 28 subcortical volumes, and 22 hippocampal subfield volumes, characteristic atrophy was detected by one-way, three-factor ANOVA and *post hoc* pairwise *t* tests. By contrast, functional connectivity analysis of 57 left hemisphere MTL and subcortical ROIs with 82 ROIs in both hemispheres, and 69 right MTL and subcortical ROIs with 120 ROIs in both hemispheres, detected significant MCI-CN changes.

[1] NuroSci, LLC. West Palm Beach, FL, 33401.
[2] Center for Complex Systems and Brain Science, Florida Atlantic University, Boca Raton, FL, 33431.
[3] Data used in preparation of this article were obtained from the Alzheimer's disease Neuroimaging Initiative (ADNI) database (adni.loni.usc.edu). As such, the investigators within the ADNI contributed to the design and implementation of ADNI and/or provided data but did not participate in analysis or writing of this report. A complete listing of ADNI investigators can be found at: http://adni.loni.usc.edu/wp-content/uploads/how_to_apply/ADNI_Acknowledgement_List.pdf.

Copyright © 2017. NuroSci, LLC.

Confirmatory findings include an anterior-posterior cortical DMN "disconnect". Novel findings include a bilateral posterior DMN disconnect and a DMN-PHG disconnect. A novel data-driven approach for ROI identification and selection was developed and implemented with the AFNI toolkit. These findings position candidate resting-state functional MRI connectivity biomarkers within a model Alzheimer's disease pathophysiological cascade as coincident with and potentially in advance of morphometric biomarkers of the CN to MCI transition.

Keywords: ageing; Alzheimer's disease; default-mode network; hippocampus; mild cognitive impairment; medial temporal lobe; neuroimaging; parahippocampal gyrus; resting-state fMRI

Abbreviations: ADNI = Alzheimer's disease Neuroimaging Initiative; CDR= clinical dementia rating; CDRSB= clinical dementia rating, sum of boxes; CDT= cluster determination threshold; CMT= color maximum threshold; CN= cognitively normal; D= dementia; DMN= default-mode network; EPI= echo-planar image; FWHM= full width half maximum; ICA= independent components analysis; ICV = intra-cranial volume; MCI = mild cognitive impairment; MMSE= mini-mental state examination; MTL= medial temporal lobe; PCC= posterior cingulate cortex; PHG = parahippocampal gyrus; rsfMRI= resting-state functional MRI; ROI= region of interest;

Running Title: Alzheimer's disease functional connectivity and morphometric changes

Introduction

In late-onset Alzheimer's disease, neuropathologies may cumulate for decades before possible though not inevitable clinical manifestation. Diagnostic guidelines (Jack, 2011; McKhann, 2011; Albert, 2011; Sperling, 2011; Vinters, 2015) for cognitively normal, mild cognitive impairment, and Alzheimer's disease consider neuroimaging biomarkers, including labelling (Amyloid PET),

Copyright © 2017. NuroSci, LLC.

metabolic (FDG PET) and morphometric (MRI) (Klunk, 2004; Fan, et al., 2008; Davatzikos, et al., 2009; Misra, et al., 2009; Jack, 2011; Sorensen, et al., 2016; Wolk, et al., 2017). Disruption of functional connectivity in Alzheimer's disease has been observed in the DMN in resting-state functional MRI (rsfMRI), a non-invasive, repeatable neuroimaging methodology (Greicius, et al., 2004; Buckner, et al., 2005; Sorg, et al., 2007; Zhou, et al., 2010; Jones, et al., 2011; Jones, et al., 2012, Brier, et al., 2012; Ward, et al., 2014; Cai, et al., 2015; Dillen, et al., 2017). However, such observations have not broadly impacted clinical practice (Woo, et al., 2017).

Here we test the hypothesis that in the absence of evidence of statistically significant CN to MCI morphometric changes, particularly in anatomical regions associated with the DMN and additional coactivated regions in MTL, functional connectivity disruptions directly involving these structures are detected. We present evidence confirming the hypothesis. We suggest that functional connectivity analysis of rsfMRI may provide a complementary approach to established neuroimaging and other biomarkers within the framework of a model of Alzheimer's disease pathophysiology (Jack, 2013).

Materials and Methods

Data used in the preparation of this report was obtained from the Alzheimer's disease Neuroimaging Initiative (ADNI) database (adni.loni.usc.edu). The ADNI project was launched in 2003 as a public-private partnership, led by Principal Investigator Michael Weiner, MD. The primary goal of ADNI has been to test whether serial magnetic resonance imaging, positron emission tomography, other biological markers, and clinical and neuropsychological assessment can be combined to measure the progression of mild cognitive impairment and early Alzheimer's disease.

SUBMISSION DRAFT – FOR REVIEW ONLY.
Copyright © 2017. NuroSci, LLC.

Clinical population

The clinical population in this report is a subset of the ADNI 2 experimental sub-study on resting state fMRI functional connectivity (rsfMRI) (Jack, et al., 2008; Weiner, et al., 2015). The ADNI 2 rsfMRI data available for download on the Laboratory of Neuro Imaging (LONI) website in September 2016 consisted of 886 scan pairs (structural MRI, rsfMRI) from 220 subjects recorded during visits over the course of the multi-year ADNI study. The paired series were processed through a multistage image and quality assurance procedure and yielded a cross-sectional study dataset consisting of one scan pair per each of 105 subjects.

Image acquisition

A typical ADNI 2 clinical visit sequence consisted of an initial screening visit, a baseline visit, a 3-month, 6-month and 12-month, and annual visit thereafter. Of interest in the present analysis are two of the up to eight scans obtained during each ADNI 2 subject visit. The scans of interest are the high-resolution T_1-weighted 3D volumetric structural scan (Scan #2 in the protocol) and resting state functional scan (Scan #4 in the protocol) obtained during each subject visit.

Whole-brain high-resolution structural images were recorded in 3T MRI scanners of a single manufacturer (Philips Medical Systems: Achieva, Ingenia, Ingenuity, Intera) from 14 unique sites in two configurations (MULTI-COIL; SENSE-HEAD), and fifteen (15) different software versions, the most common being 3.2.1 or higher. The ADNI structural scan protocol defined a T_1-weighted sagittal magnetization-prepared rapid gradient echo (MP-RAGE) scan. Typical parameters extracted from ADNI XML metadata files were: a) flip angle, 9°; b) volume; 256 x 256 x 170; c) pixel spacing, 1.0 mm; d) slice thickness, 1.2 mm; e) TE (3.14 msec) and f) TR (6.77 msec).

Copyright © 2017. NuroSci, LLC.

The rsfMRI scan protocol defined a T_2-weighted sequence. Typical parameters extracted from ADNI XML metadata files were: a) flip angle, 80°; b) pixel spacing, 2.79 - 3.313 mm; c) slice thickness, 3.312 mm; d) TE=30.0 msec; e) TR=3000 msec; and f) phase-direction (anterior-posterior, N=16; posterior-anterior, N=86; missing values=4). Only two (of nine observed) temporal slice order sequences were admitted to the present 105 scan dataset: a) ascending 48 planes (odd, even), N=98; and b) descending 48 planes (even, odd), N=7. rsfMRI scans were of two durations: a) 140 TRs ("resting state", N=91); and b) 200 TRs ("extended resting state", N=14). The scans with 200 TRs were truncated to 140 TRs for the final stage functional connectivity analysis.

Image processing

Structural images and rsfMRI images were downloaded from LONI either in DICOM format (and locally converted using dcm2nii) or in 4DNIfTI format (whereby the DICOM to NIfTI conversion was completed by LONI). Preprocessing and data analysis were performed using a combination of FreeSurfer (Dale, et al., 1999), Analysis of Functional Neuroimages (AFNI) (Cox, 1996), and "home-grown" analysis implemented in R and *tcsh* shell scripts. The AFNI Version was AFNI_17.1.03 (2-May-2017). The FreeSurfer version was V6.0 and was run in the Amazon Cloud on Ubuntu 14.04. The R version was Version 3.2.3 (10-Dec-2015). The AFNI Python script uber_subject.py was used to generate a preprocessing shell script which was manually edited.

Structural image analysis with FreeSurfer 6.0

Subcortical and hippocampal subfield segmentation, and cortical parcellation (surface area, thickness and volume) were obtained with FreeSurfer Version 6.0 image analysis suite, which is

Copyright © 2017. NuroSci, LLC.

documented and freely available for download online (http://surfer.nmr.mgh.harvard.edu/) (Dale, et al., 1999). FreeSurfer default settings were applied via the "recon-all" command.

Functional MRI analysis with AFNI

The rsfMRI EPI preprocessing sequence consisted of the following steps in AFNI: a) alignment of EPI centers to a standard atlas; b) elimination of the first two EPIs; c) outlier detection and de-spiking; d) application of time-shift correction; e) alignment of each EPI to the least motion distorted volume; f) alignment to the anatomical image and nonlinear warp to a standard space (MNI_avg152T1); g) generation of anatomical and EPI masks; h) application of spatial smoothing (FWHM = 4.0mm); i) scaling each voxel time series to a mean of 100; j) generation of demeaned motion parameters and motion parameter derivatives; k) generation of motion "censor" masks (motion limit = 0.3); l) generation of ventricle (Vent) and white-matter segmentation masks from FreeSurfer segmentation and parcellation results; and m) deconvolution with 12 regressors (6 regressors + 6 motion derivatives). The process yielded a 4D residual error volume that served as input to the next stage of volumetric and correlation analysis. The global average signal was not removed from 4D volumes and there was no bandpass filtering in the preprocessing stage.

Image quality assurance

The starting database consisted of 886 rsfMRI scans (and their paired structural images) downloaded from LONI. An R package "ADNIMERGE" contained MRI and rsfMRI quality assessments (e.g., comments by ADNI quality reviewers) and related data (e.g., rsfMRI slice order) stored in the tables "mayoadirl_mri_imageqc" and "mayoadirl_mri_fmri", respectively. The 886-scan set (n=220 subjects) was reduced to 673 scans (n=196) by rejecting all scans that

Copyright © 2017. NuroSci, LLC.

did not conform to the slice order sequences noted above, or had clearly excessive motion based on visual inspection in the FSL viewer, or contained any reviewer comment in either of the available pair of comment fields. Comments typically referenced motion or clinical findings.

The rsfMRI EPI preprocessing sequence with motion-limit set to 0.3 was applied to each of the 673 structural-rsfMRI pairs. The global average signal of the rsfMRI scan was analyzed as an initial screen for excessive motion. Scans were rejected if the global average time-series amplitude value fell outside the range 96-104 or that the standard deviation of the global average time series exceeded 2.0. The gross motion screening procedure reduced the 673 structural-rsfMRI pairs database to 507 (n=190 subjects).

The 507 scan pairs database was further screened using statistics generated by the AFNI-based preprocessing pipeline. Scans were marked for rejection according to the following criteria: a) DICE coefficient < 0.78; b) censor fraction > 0.21; c) maximum censored displacement > 1.00; d) average TSNR > 400 or average TSNR < 100; e) degrees of freedom left < 100; and f) global correlation > 0.11. 206 scan pairs from 106 subjects met these quality assurance criteria. The final dataset reduction step enforced the rule of a single scan pair per subject: 105 structural-functional scan pairs from 105 subjects. Where multiple candidate scan pairs were present, the latest available pair was selected: 80% of the final dataset consists of data recorded from subjects who were on at least their second ADNI 2 study visit. ANOVA confirmed that preprocessing quality measures were matched across the three diagnostic groups.

Seed ROI definition

ROI seeds were defined by an anatomically bootstrapped data-driven procedure. The procedure was applied independently to the left and right hemispheres. To bootstrap the ROI seed selection

Copyright © 2017. NuroSci, LLC.

procedure, FreeSurfer subcortical segmentations were used to define the 3D bounding box for the hippocampus and MTL. A grid of 6mm-spaced coordinates within the bounding box formed the input candidate ROI seed pool. The input candidate seeds that supported a complete 6mm radius spatial sample (33 voxels), determined by comparison with the global brain mask generated during AFNI baseline processing, formed a base set of anatomical ROI seeds.

To define corresponding paired ROI seeds, we performed the following volumetric ROI procedure on each base set ROI seed. First, for each base set ROI seed, compute and retain the subject-dependent average time series from the 6mm radius sphere centered at the ROI seed. Second, compute the Fischer z-transformed Pearson correlation coefficient between subject averaged time series and every other voxel in the subject 4D image (restricting the computations to those voxels contained within the global brain mask generated during AFNI baseline processing). Third, with the resulting set of subject-dependent 3D Fischer z-transform volumes, conduct a group-level, one-way, three-factor (CN, MCI, Dementia) 3D ANOVA at each voxel and retain the 3D volume of F statistics. Fourth, perform a 3D cluster analysis on the F statistic 3D volume and retain the coordinate of the center of mass (expressed as a 3D integer valued coordinate) of each qualified cluster as a base ROI-dependent candidate paired ROI seed. Retain as well as each cluster extent (number of voxels) and weight (F statistic averaged over cluster extent). Cluster determination threshold ($F \geq 4.816$; $p \leq 0.01$, uncorrected) and minimum cluster size ($N_C = 20$) were chosen to be permissive by design. Fifth, combine the outputs of the previous stage across all base ROI seeds and retain as the raw list of paired ROI seed candidates. Prune the raw list of paired ROI coordinates such that the minimum distance between the paired ROI seeds is > 6mm. For each paired ROI, compute and retain the subject-dependent average time series from the 6mm radius sphere centered at the paired ROI seed.

Copyright © 2017. NuroSci, LLC.

The anatomically bootstrapped, data-driven ROI definition procedure yielded per subject for the left hemisphere a total of 139 ROI seeds and corresponding spatially averaged time series, and per subject for the right hemisphere a total of 189 ROI seeds and corresponding spatially averaged time series. Anatomically-bootstrapped ROI seeds were hemisphere-specific, but paired ROI seeds ranged over both hemispheres. These time series were subjected to additional quality assurance checks and input to a pairwise ROI cross-correlation analysis described next.

ROI time series quality assurance

Prior to inclusion in pairwise correlation analysis individual ROI average time series were subjected to band-pass filtering (4th order Butterworth, $f = \{0.01, 0.1\}$) and a final quality assurance check for outliers. The 3rd-138th time series elements were retained as the candidate final ROI time series. For subject *k*, ROI *j*, the time series was rejected if any of the following conditions were true: a) the time series was constant; b) the time series standard deviation, $\sigma_{jk} > 20.0$; or c) the fraction of time points with values greater than the outlier threshold θ_{jk} exceeded 5%. The outlier threshold was set as $\theta_{jk} = \mu_{jk} + 3\sigma_{jk}$, where μ_{jk} is the time series average. Rejected time series counts and percentages were as follows: a) left CN, 8 of 4,448 (0.18%) from 3 subjects; b) left MCI, 8 of 5,421 (0.15%) from 5 subjects; c) left D, 13 of 4,726 (0.28%) from 7 subjects; d) right CN, 15 of 6,048 (0.25%); e) right MCI, 11 of 7,371 (0.14%); and f) right D, 18 of 6,426 (0.28%). Rejected time series resulted in NA entries in the corresponding subject ROI Pearson correlation coefficient matrices. These NA entries propagated into the ANOVA stage as subject missing values. For the set of 9,591 left hemisphere ANOVA tests, 9,443 (98.5%) included at least 102 of 105 subjects (97.1%) as did 100% of the significant ANOVA tests and 100% of the significant *post hoc* pairwise *t* test MCI-CN contrast tests discussed in Results. For the set of 17,766 right hemisphere ANOVA tests, 17,018 (95.8%) included at least 102 of 105

Copyright © 2017. NuroSci, LLC.

subjects (97.1%) as did 100% of the significant ANOVA tests and 100% of the significant *post hoc* pairwise *t* test MCI-CN contrast tests discussed in Results.

ROI pairwise correlation analysis

Pairwise correlation analysis was at the level of individual ROI pairs. The core statistical method was one-way, three-factor (clinical assignment) ANOVA, with *post hoc t* tests applied pairwise only for significant ANOVA tests, correcting for large-scale multiple testing through False Detection Rate correction (Benjamini & Hochberg, 1995) and permutation repeated measures (Nichols and Holmes, 2002; Efron, 2010; Eklund, et al., 2016).

Assignment of anatomical position to an ROI coordinate

For expository purposes, we mapped ROI seed MNI coordinates to anatomical locations by analyzing the output of the AFNI *whereami* output. The AFNI *whereami* tool maps an input coordinate to anatomical position with respect to a multiplicity of atlases. To assign a final anatomical label we used the “Focus Point”, and “Within 2mm” or “Within 4mm” outputs from the Talairach-Tournoux, MNI (Macro Labels, N27), and MNI (Cytoarchitectonic Max Probability Maps) and checked for consistency. Results were visually confirmed.

Results

Clinical population

The clinical population in this report is a subset of the ADNI 2 sub-study on resting state fMRI (rsfMRI) (Supplementary Table 1). Subjects were assigned to one of three clinical categories: Cognitively Normal (CN; N=32; median age=73.3); Mild Cognitive Impairment (MCI; N=39; median age=72.4); and Dementia (D; N=34; median age=74.6). Except where noted, the term

Copyright © 2017. NuroSci, LLC.

"dementia" used in this analysis refers to mild dementia. Clinical assignments followed ADNI 2 protocols determined by individual patient CDR, CDRSB and MMSE scores. CN was defined as CDR 0, CDRSB 0, and MMSE ≥ 24. MCI was defined as CDR 0.5 and MMSE ≥ 24.0. D was defined as 0.5 ≤ CDR ≤ 1.0 and 20 ≤ MMSE ≤ 26. ANOVA confirmed that age, education and gender were matched, but that APOEϵ4(2) status was not matched (CN: 3% of CN; MCI: 10%; D: 26%).

Structural MRI analysis

Structural MRI analysis was performed using the FreeSurfer Version 6.0 image analysis suite (http://surfer.nmr.mgh.harvard.edu/). The effect of clinical category on cortical thinning was evaluated using one-way, three-factor ANOVA on estimates of cortical thickness from 34 cortical regions per hemisphere (68 total) (Supplementary Table 2). An ANOVA F statistic $p <$ 0.05 value, p_F^*, corrected by the False Discovery Rate (FDR), q=0.1, gave $p_F^* = 0.032$ and identified 23 significant tests. For significant ANOVA tests only, *post hoc* pairwise *t* tests were computed and then FDR-corrected for three comparisons: MCI-CN ($p_{MCI,CN}^*$=0.006), D-CN ($p_{D,CN}^*$=0.037), and D-MCI ($p_{D,MCI}^*$=0.022). There were no significant negative MCI-CN comparisons. There were two significant positive MCI-CN comparisons (left and right paracentral lobule), though each changed the group average by less than 4.4%. By contrast, there were twenty-one significant D-MCI comparisons and fifteen significant D-CN comparisons. Effect sizes, measured by Cohen's d, were in the range $0.6 \leq d \leq 1.0$. Consistent with existing evidence of cortical thinning in Alzheimer's disease, all D-MCI and D-CN contrasts were negative.

Copyright © 2017. NuroSci, LLC.

The effect of clinical category on subcortical volumes was evaluated using one-way, three-factor ANOVA on estimates from eight regions per hemisphere (16 total) (Supplementary Table 3). Values were normalized by the estimated total intracranial volume. The FDR-corrected (q=0.1) ANOVA F statistic p value, p_F^* = 0.012, identified eight significant tests. For the significant ANOVA tests only, *post hoc* pairwise t tests were computed and FDR-corrected for the contrasts D-CN ($p_{D,CN}^*$ = 0.004), and D-MCI ($p_{D,MCI}^*$ = 0.031). For the MCI-CN contrast no p value fell below the FDR-corrected level indicated by q=0.1. Thus, we list the FDR-corrected p value as "not applicable" ($p_{MCI,CN}^*$ = NA) and conclude that there were no significant MCI-CN comparisons. There were eight significant D-CN contrasts; and six significant D-MCI contrasts. Effect sizes were in the range $0.3 \leq d \leq 1.1$. All significant pairwise comparisons for ventricles (e.g., inferior lateral ventricle) were positive and all significant pairwise contrasts for subcortical structures (e.g., hippocampus) were negative, consistent with Alzheimer's disease progression.

Hippocampal sub-fields (11 per hemisphere) were analyzed similarly as above and all twenty-two ANOVA tests were significant, FDR corrected p value (q=0.1), p_F^* = 0.032 (Supplementary Table 4). *Post hoc* pairwise t tests detected twenty-two significant D-CN comparisons ($p_{D,CN}^*$ = 0.029), and eighteen significant D-MCI comparisons ($p_{D,MCI}^*$ = 0.077). Effect sizes, measured as Cohen's d, were at least "strong" and above, with left hemisphere effect scores uniformly higher than the right hemisphere (left: $0.9 \leq d \leq 1.1$; right: $0.7 \leq d \leq 0.86$). Consistent with Alzheimer's disease progression all significant D-MCI and D-CN hippocampal sub-field pairwise contrasts were negative. For the MCI-CN comparison, however, no p value fell below the FDR-corrected level indicated by q=0.1. Thus, we list the FDR-corrected p value as "not applicable" ($p_{MCI,CN}^*$ = NA) and conclude that there were no significant MCI-CN comparisons.

Copyright © 2017. NuroSci, LLC.

ROI pairwise functional connectivity

Here we present evidence in support of the hypothesis that in the absence of evidence of statistically significant CN to MCI morphometric changes, functional connectivity disruptions directly involving these structures are detected. We tested the hypothesis separately for the left and right hemispheres with a focus on the MCI-CN contrast. Using an automatic, data-driven procedure described above in Methods, we identified 57 ROI seeds in the region of left hippocampus and adjacent structures (e.g., medial temporal lobe (MTL), thalamus), and a corresponding set of 82 ROI seeds in both left and right hemispheres (total N=139 ROIs). Similarly, we identified 69 ROI seeds in the region of right hemisphere hippocampus and adjacent structures, and a corresponding set of 120 ROI seeds in both hemispheres (total N=189 ROIs). Functional connectivity analysis consisted of the evaluation of the effect of clinical category on group-level ROI-ROI pair-wise time series correlations (Fisher Z transformed Pearson correlation coefficient), where for each ROI we computed the average time series over the voxels (N=33) contained in a 6mm sphere centered on the ROI seed.

The effect of clinical category on group average ROI-ROI pair-wise correlation was evaluated using one-way, three-factor ANOVA. The sample p value for each ANOVA test was validated using repeated measures (5000 random permutation trials of sample data clinical category labels) and counting the proportion of repeated trials in which the resampled F statistic was greater than the sample F-statistic) (Nichols and Holmes, 2002; Efron, 2010; Eklund, et al., 2016). Correction for multiple comparisons was performed with FDR correction (q = 0.05) over the set of sample p values (left: N = 9,591 tests; right: N = 17,766 tests).

Left hemisphere ROI analysis

Copyright © 2017. NuroSci, LLC.

There were twenty-one significant ANOVA tests found using the FDR-corrected F-statistic $p < 0.05$ value ($p_F^* < 0.0002$). *Post hoc* pairwise *t* tests were performed only for the significant ANOVA tests for each of three contrasts: MCI-CN; D-CN; and D-MCI. The contrast sample *t* test *p* values were computed and validated as part of the resampling procedure above and correction for multiple comparisons was with FDR ($q = 0.05$) over the set of twenty-one tests per contrast: $p_{MCI,CN}^* = 0.0140$; $p_{D,CN}^* = 0.0280$; $p_{D,MCI}^* = 0.0196$.

Of the twenty-one significant ANOVA comparisons, there were seven significant *post hoc* MCI-CN *t* test comparisons (*post hoc* pairwise *t* test $p < p_{MCI,CN}^*$) (Fig. 1a, Supplementary Table 5). All seven of the comparisons were negative meaning that group average CN functional connectivity was greater than in MCI. Of these seven significant MCI-CN comparisons, there was one intrahemispheric comparison (ROI seed pair) ($p = 0.0066$, Cohen's d=0.60, moderate effect size) for MNI coordinate (-17, 67, 1), superior frontal gyrus (Brodmann Area 10), and MNI coordinate (-40, -76, 29), superior occipital gyrus (Brodmann Area 19). Six of the seven significant MCI-CN comparisons were between left and right hemisphere ROIs, and they had moderate to strong effect size ($0.55 \leq d \leq 1.0$, median $d = 0.78$).

Spatial correlation maps corresponding to representative significant ROI pairs are shown in Figure 2. In Figure 2 the ROI seed is centered at (-14, -44, 4) in the region of left parahippocampal gyrus and Brodmann Area 30 (posterior cingulate cortex). The paired ROI is centered at (7, -62, 8) (right cuneus and Brodmann Area 30). The MCI-CN ROI pairwise *t* test is $p = 0.0140$ and the effect size is moderate ($d = 0.55$). The results shown are notable for several reasons. First, the anatomical positions of this ROI pair align with Default Mode Network (DMN) nodes. Second, the ROI pair was identified in a data driven fashion with minimal researcher guidance. Last, the statistically significant reduction in group average functional

Copyright © 2017. NuroSci, LLC.

connectivity in the MCI-CN contrast is significant as well in the D-MCI and D-CN contrasts. These results demonstrate a monotonic decrease in functional connectivity with Alzheimer's disease progression between the left posterior hippocampal-parahippocampal region and the right cuneus-posterior cingulate cortex.

We observed a functional disconnect between an anterior subcortical (thalamus) and a posterior cortical region associated with the DMN (Fig 1a; Supplementary Table 5; Extended Data Figure 1). The ROI seed was centered at (-6, -12, 4) in the region of left medial dorsal nucleus and ventral lateral nucleus of the thalamus. The paired ROI was centered at (48, -69, 36) (right angular gyrus, Brodmann Area 39, and inferior parietal cortex). The MCI-CN ROI pairwise *t* test was $p < 0.001$ and the effect size was strong ($d = 0.99$).

Additional significant ROI pairs in the MCI-CN contrast (Supplementary Table 5) were: a) left caudate tail and hippocampus (CA) seed with paired ROI in the region of right posterior superior temporal and medial gyri, and the inferior parietal cortex ($p < 0.001$, $d = 1.02$); b) a more lateral ROI in left caudate tail and hippocampus (CA) and a paired ROI in the region of right posterior cingulate cortex ($p < 0.001$, $d = 0.86$); and c) an ROI in the region of the left parahippocampal gyrus and Brodmann Area 36 (perirhinal cortex) and a paired ROI in the region of the right caudate (head), ($p = 0.002$, $d = 0.70$).

The observation of significant contrasts in MCI-CN functional connectivity shown in Figure 1a was validated using repeated measures (N = 5000 trials) procedures that permuted group labels. There were no significant randomized ANOVA tests or *post hoc* pairwise *t* tests (Fig. 1b).

We next assessed the effect of Alzheimer's disease progression on the D-MCI contrast (Supplementary Table 5). Of the seven significant MCI-CN ROI (Fig. 1a), two did not have

Copyright © 2017. NuroSci, LLC.

significant D-MCI contrast, four had significant positive D-MCI contrast, and one had significant negative D-MCI contrast (Figure 1a). Overall, twelve of twenty-one ANOVA significant ROI pairs were significant and *positive* for the D-MCI contrast (Fig. 1c) and seven of twenty-one ANOVA significant ROI pairs were significant and *negative* for the D-MCI contrast (Fig. 1d). These results are evidence of monotonic and non-monotonic changes in functional connectivity between ROI pairs with Alzheimer's disease progression.

Right hemisphere ROI seeds

With an FDR corrected F statistic $p < 0.05$ value ($p_F^* < 0.0002$) there were nineteen significant ANOVA tests (out of 17,766 tests). *Post hoc* pairwise *t* tests were performed only for the significant ANOVA tests for each of three contrasts: MCI-CN; D-CN; and D-MCI. The contrast sample *t* test *p* values were validated as part of the resampling procedure above and correction for multiple comparisons was with FDR (q=0.05) over the set of nineteen tests per contrast: $p_{MCI,CN}^* = 0.0102$; $p_{D,CN}^* = 0.0394$; $p_{D,MCI}^* = 0.0088$.

For the MCI-CN contrast, there were thirteen significant comparisons (ROI pairs) (*post hoc* pairwise *t* test $p < p_{MCI,CN}^*$) (Fig. 3a, b; Supplementary Table 6). There was one positive MCI-CN contrast ($p < 0.001$, $d = 1.0$): seed (38, -4, -28) in the region of right inferior and medial temporal gyrus and hippocampus (CA); paired ROI seed (24, -22, 73) in a region between right precentral and postcentral gyri (Figure 3a). There were twelve negative MCI-CN contrasts with *p* values in the range $p_{MCI,CN}^* < 0.0001$ to $p_{MCI,CN}^* < 0.0102$, median $p_{MCI,CN}^* = 0.0007$, and Cohen's *d*, $0.55 \leq d \leq 1.37$, median $d = 0.81$ (Figure 3b). Of these twelve negative contrasts, five consisted of a cross-hemispheric ROI pair; the remaining seven were right intrahemispheric.

Copyright © 2017. NuroSci, LLC.

Spatial correlation maps corresponding to a representative significant ROI pair are shown in Figure 4. In Figure 4 the seed ROI is at (34, -36, -8) in the region of right fusiform gyrus, parahippocampal gyrus, and hippocampus (CA). The paired ROI is centered at (6, -54, 52) in the region of right precuneus, Brodmann Area 7, and superior parietal lobe. The MCI-CN ROI pairwise *t* test is $p = 0.0074 < p^*_{MCI,CN}$ the effect size is moderate ($d = 0.60$). These right hemisphere results, taken together with similar observations for left hemisphere, provide evidence of an interhemispheric "disconnect" between posterior MTL and DMN posterior cortical regions.

There is also evidence of interhemispheric disconnection between right anterior subcortical and posterior ventral cortical regions associated with the DMN, comparable to that observed for the left hemisphere. Specifically, one significant MCI-CN ROI pair *t* test was $p < 0.001$ and the effect size was strong ($d = 1.1$). One ROI was centered at (12, -14, 0) in the right ventral lateral nucleus of the thalamus; the paired ROI was centered at (34, -6, -28) (inferior and middle temporal gyri, hippocampus (EC, SUB)).

Additional significant MCI-CN ROI pairs are as follows: a) seed region in the right ventral anterior nucleus of the thalamus, paired region in the left superior frontal gyrus and supplementary motor area (SMA) ($p < 0.001$, $d = 1.38$); b) seed region right posterior cingulate cortex and hippocampus (CA), paired region left middle temporal gyrus and Brodmann Area 22 ($p < 0.01$, $d = 0.60$); c) seed region right parahippocampal gyrus, Brodmann Area 19 and 37, paired region *left* cerebellum (VIIIa, b) ($p < 0.001$, $d = 1.02$); and d) the same seed region as in (c), paired region *right* cerebellum (VII, VIIb) ($p < 0.001$, $d = 0.80$). In every case listed above, the paired ROIs are within a region associated with the DMN (e.g., hippocampus, cingulate cortex, cerebellum) or other resting state network (e.g., SMA).

SUBMISSION DRAFT – FOR REVIEW ONLY.
Copyright © 2017. NuroSci, LLC.

We assessed the effect of Alzheimer's disease progression in the D-MCI contrast. Of the twelve significant MCI-CN comparisons, three did not have significant D-MCI contrast, eight had significant positive D-MCI contrast, and one had significant negative D-MCI contrast. Overall, nine of nineteen significant ANOVA comparisons (ROI pairs) were significant and *positive* for the D-MCI contrast (Fig. 3c) and six of nineteen significant ANOVA comparisons were significant and *negative* for the D-MCI contrast (Fig. 3d).

Discussion

Sensitivity analysis

In preliminary studies, we assessed through spot-checking the sensitivity of the detection of statistically significant (one-way, three-factor ANOVA ROI pair) functional connectivity comparisons to changes in preprocessing parameters. The results reported in this study were obtained with FWHM = 4.0 mm spatial smoothing in the AFNI preprocessing stage. Smoothing with FWHM = 6.0 mm or FWHM = 8.0 mm, and FDR q value (0.05), eliminated the observation of significant ANOVA trials. In such cases, we did not proceed to the 5000 permutation repeated measures test (although we observed anecdotally using a 1000 permutation repeated measures test that a few significant tests were observed). Similarly, present results were obtained using an ROI defined as the 6.0 mm radius volume centered at a given source or target ROI seed. Expansion to an 8.0 mm radius volume, all else being equal, eliminated the observation of significant ANOVA tests. In any of the above tests, when we relaxed the FDR q value, for example, to $0.10 \leq q \leq 0.20$, progressively greater numbers of significant ANOVA

Copyright © 2017. NuroSci, LLC.

tests were observed. These preliminary observations drove the decision to proceed with FWHM = 4.0 mm and ROI volume radius = 6.0 mm where, with a conservative FDR q = 0.05.

We assessed the reproducibility of the reported results under repeated measures with different random number generator seeds in the 5000-trial permuted repeated measures. We completed two additional 5000-trial runs for the left hemisphere data and found that for the MCI-CN contrast (the only contrast analyzed in detail) there were comparable numbers of significant tests, ~2/3 were the same ROI pairs with comparable F statistic values to those reported here. The remaining pairs were typically in positions adjacent to or nearby those reported.

Finally, for the reported pairwise ROI functional connectivity results we determined the impact of an even more conservative FDR value q = 0.01. We analyzed results only for the left hemisphere. The FDR corrected F statistic p value was ($p_F^* < 0.0001$) and there remained 21 significant ANOVA tests. *Post hoc* pairwise t tests were performed only for the significant ANOVA tests for each of three contrasts: MCI-CN; D-CN; and D-MCI. The contrast sample t test p values were computed and validated as above and correction for multiple comparisons was with FDR (q = 0.01) over the set of 21 tests per contrast: $p_{MCI,CN}^* = <0.0001$; $p_{D,CN}^* = 0.0044$; $p_{D,MCI}^* = 0.0024$. There were three significant MCI-CN pairs, all negative (indicating loss of connectivity), and all with strong Cohen's d effect size, d > 0.86. All three were left source ROI and right target ROI: a) left thalamus (medial dorsal nucleus), right angular gyrus; b) left hippocampus (CA in region of caudate tail), right superior temporal gyrus, inferior parietal cortex; and c) left hippocampus (CA in region of caudate tail), right posterior cingulate cortex.

Comparison to previous work

Copyright © 2017. NuroSci, LLC.

Six published reports are particularly relevant to the present study (Grecius, et al., 2004; Jones, et al, 2011; Brier, et al., 2012; Ward, et al., 2014; Dillen, et al., 2017; Wolk, et al., 2017). Grecius, et al., (2004) performed a pairwise group-level (healthy control (N=14) vs very mild or mild Alzheimer's disease (N=13)) ICA and ROI analyses of steady-state DMN connectivity during a simple sensorimotor task in a cohort drawn the Washington University Alzheimer's disease Research Center. Key findings were: a) prominent bilateral coactivation of the hippocampus with DMN in both clinical groups; and b) disruption of hippocampal – PCC connectivity in the Alzheimer's disease group. Dillen et al., (2017) performed a within-group and between-group analysis of hippocampus and DMN node functional connectivity analysis in a cohort drawn from an outpatient population at the Memory Clinic Cologne Julich (healthy control (N=25), subjective cognitive decline (N=28); and prodromal Alzheimer's disease (N=25)). Significantly, they reported a decoupling of hippocampus with posterior cortical DMN nodes in SCD and prodromal Alzheimer's disease groups.

Present results demonstrate bilateral coactivation of hippocampus with task-free DMN and disruption of MTL – PCC functional connectivity, particularly in the MCI-CN comparison. We note that present results were obtained in a multi-site, multi-investigator Alzheimer's disease dataset and with independent statistical methods. Present results extend previous findings in two ways. First, the hippocampal – PCC disconnection is observed as part of a larger pattern of left-right hemisphere disconnection amongst DMN nodes. Second, group-level disruption of functional connectivity in MCI-CN is observed in a cohort in which *there were no statistically significant morphometric MCI-CN comparisons recorded in any of the measured hippocampal subfields.*

Copyright © 2017. NuroSci, LLC.

Brier, et al., (2012) performed a cross-sectional analysis of five task-free resting state networks (RSN), including DMN, in a cohort drawn from the Knight Alzheimer's disease Research Center at Washington University in St. Louis. Subjects were assigned to one of three groups according to CDR scores 0 (cognitively normal, N=386), 0.5 (very mild AD, N=91), and 1.0 (mild AD, N=33). The authors derived summary measures of intranetwork, internetwork steady-state correlation structure based on Fisher z-transformed pairwise Pearson correlation analysis of ROI seed-based average time series. While not uniformly statistically significant, the conclusion was that at the group level there was of a progressive loss of intranetwork and internetwork connectivity. The authors also reported results of the effect of clinical group on ROI pair-wise functional connectivity between PCC and eight other DMN nodes. For two ROI pairs (PCC – medial prefrontal cortex; PCC –left inferior temporal lobe) there was a statistically significant reduction of connectivity in the CDR 0.5 group compared to the CDR 0 group. Present results confirm the Brier, et al., observation of ROI pair-wise functional connectivity loss in the MCI-CN comparison. Present findings extend Brier, et al., results in several ways. First, where Brier, et al., utilized a single ROI seed to estimate midline DMN structures (e.g., PCC, thalamus), the present study utilized an anatomically bootstrapped data-driven method that identified distinct left and right ROI seeds in these structures. The result was a relatively more fine-grained ROI pair-wise analysis which led to the observation of widespread left- and right-hemispheric disconnect amongst DMN and DMN coactivated regions. We observed, in addition, disconnection between subcortical and cortical structures. Second, again leveraging the above ROI identification and selection procedure, the present study included hippocampus and other MTL structures in the analysis and presented evidence that these structures are implicated in the loss of functional connectivity in the MCI-CN comparison. Last, as noted above, the present

Copyright © 2017. NuroSci, LLC.

results were obtained in a multi-site, multi-investigator database and in which no statistically significant morphometric changes were observed in the MCI-CN comparison.

Jones, et al. (2011) performed group-level functional connectivity analyses of task-free steady-state DMN connectivity in cohorts drawn from the Mayo Clinic Alzheimer's disease Research Center and Mayo Clinic Study of Aging. Age-related changes in DMN functional connectivity were analyzed using an ICA approach in a cognitively normal cohort (N=341). The age-related changes consisted of differential effects in anterior and posterior DMN connectivity: a) anterior DMN showed both increases and decreases in connectivity within the frontal lobe; and b) posterior DMN showed a pattern of mainly, but not exclusively, decreases in connectivity. An age-matched CN and Alzheimer's disease group analysis using both ICA and seed-based ROI approaches concluded that DMN connectivity changes in Alzheimer's disease represent an acceleration of the same aging pattern observed in the control sample. Present results confirm and extend observations of a diversity of functional connectivity decreases (in the CN to MCI transition) and increases (particularly in the MCI to D transition) within the DMN, including subcortical-cortical disconnection and bi-lateral disconnection.

Ward, et al., (2014), in their study comparing resting state data and an associative memory encoding task, concluded that the parahippocampal gyrus is the primary hub of the DMN in the MTL during resting state. Their report ends with the suggestion that measuring PHG connectivity may provide a biomarker of early Alzheimer's disease. The present study, although motivated by a different hypothesis (that functional connectivity changes temporally precede detection of significant neurodegeneration) and using an entirely independent analysis method (anatomically bootstrapped, data-driven method that reduces researcher degrees of freedom), to provides quantitative evidence in support of the Ward, et al., suggestion. We observe evidence

Copyright © 2017. NuroSci, LLC.

of functional disconnection bilaterally between posterior cortical DMN nodes (PCC, precuneous) and PHG as part of a larger pattern of disruption involving anterior and posterior DMN, and subcortical structures including hippocampus, thalamus and PHG. Particularly with respect to utility as a biomarker, we observed independently in the left and right PHG disconnection that was monotonic with respect to the progression from CN to MCI to Alzheimer's disease (See Figures 1 and 3, single-headed arrows).

The absence of significant morphometric changes in cortical thickness, whole hippocampus volume and hippocampal subfield volumes in the cohort reported above is with respect to a widely available benchmark: up-to-date automated analysis (FreeSurfer) of research quality T1-weighted scans (1.0 x 1.0 x 1.0 mm^3). We do not conclude that there are no morphometric changes taking place contemporaneously with the CN to MCI transition. Wolk, et al. (2017) analyzed high resolution (~0.4 x 0.4 x 2 mm^3) T2-weighted MRI scans orthogonal to the long axis of the hippocampus. They reported significant group-level reduction of hippocampal subfield volumes (e.g., Brodmann Area 35, perirhinal cortex) in the CN to early MCI transition where whole hippocampus volumes were not significantly different. The Wolk, et al., study together with present results indicates the potential of dual functional and morphometric biomarkers of the earliest stages in the Alzheimer's disease pathophysiology.

Conclusion

We report evidence in support of the hypothesis that disruption of task-free resting state network functional connectivity is present in advance of the Alzheimer's disease pathophysiological stage at which neurodegeneration has sufficiently progressed to be detected in an automated analysis of standard (1mm) structural T1 MRI as cortical thinning, subcortical structural volume reduction and hippocampal subfield volume reduction. An anatomically bootstrapped, data-

Copyright © 2017. NuroSci, LLC.

driven procedure identified statistically significant MCI-CN comparisons in resting state network ROI pairs whose anatomical locations corresponded mainly with DMN nodes. Further, we observed a diversity of effects of Alzheimer's disease progression on ROI pairwise functional connectivity including complex patterns of decreases *and* increases across the MCI-CN and D-MCI transitions suggesting that the effect of Alzheimer's disease progression on functional connectivity may be more complex than simply monotonic loss of functional connectivity.

SUBMISSION DRAFT – FOR REVIEW ONLY.
Copyright © 2017. NuroSci, LLC.

Acknowledgements

Data collection and sharing for this project was funded by the Alzheimer's disease Neuroimaging Initiative (ADNI) (National Institutes of Health Grant U01 AG024904) and DOD ADNI (Department of Defense award number W81XWH-12-2-0012). ADNI is funded by the National Institute on Aging, the National Institute of Biomedical Imaging and Bioengineering, and through generous contributions from the following: AbbVie, Alzheimer's Association; Alzheimer's Drug Discovery Foundation; Araclon Biotech; BioClinica, Inc.; Biogen; Bristol-Myers Squibb Company; CereSpir, Inc.; Cogstate; Eisai Inc.; Elan Pharmaceuticals, Inc.; Eli Lilly and Company; EuroImmun; F. Hoffmann-La Roche Ltd and its affiliated company Genentech, Inc.; Fujirebio; GE Healthcare; IXICO Ltd.; Janssen Alzheimer Immunotherapy Research & Development, LLC.; Johnson & Johnson Pharmaceutical Research & Development LLC; Lumosity; Lundbeck; Merck & Co., Inc.; Meso Scale Diagnostics, LLC.; NeuroRx Research; Neurotrack Technologies; Novartis Pharmaceuticals Corporation; Pfizer Inc.; Piramal Imaging; Servier; Takeda Pharmaceutical Company; and Transition Therapeutics. The Canadian Institutes of Health Research is providing funds to support ADNI clinical sites in Canada. Private sector contributions are facilitated by the Foundation for the National Institutes of Health (www.fnih.org). The grantee organization is the Northern California Institute for Research and Education, and the study is coordinated by the Alzheimer's Therapeutic Research Institute at the University of Southern California. ADNI data are disseminated by the Laboratory for Neuro Imaging at the University of Southern California.

Copyright © 2017. NuroSci, LLC.

Supplementary material

1. **Supplementary Information Table 1 (ADNI RID fMRI MRI DX).**

   Excel table containing ADNI subject ID, unique structural MRI image ID, unique rsfMRI image ID, and the clinical category assigned in this analysis. An authorized ADNI user will be able to access the same raw data used as a starting point in this study.

2. **Supplementary Information Table 2 (Cortical Thickness ANOVA Results)**

   Excel table containing the ANOVA F statistic and *p* value, *post hoc* pair-wise *t* statistic and *p* value, pair-wise Cohen's *d*, group average, and group average standard error, for 68 cortical region thickness estimates.

3. **Supplementary Information Table 4 (Subcortical Segmentation ANOVA Results)**

   Excel table containing the ANOVA F statistic and *p* value, *post hoc* pair-wise *t* statistic and *p* value, pair-wise Cohen's *d*, group average, and group average standard error, for 16 hippocampal subfield volume estimates.

4. **Supplementary Information Table 3 (Hippocampal Subfields ANOVA Results)**

   Excel table containing the ANOVA F statistic and *p* value, *post hoc* pair-wise *t* statistic and *p* value, pair-wise Cohen's *d*, group average, and group average standard error, for 22 subcortical structure volume estimates.

5. **Supplementary Information Table 5 (Left Hemisphere Source ROI MCI-CN Contrast ANOVA Results)**

   Excel table containing left significant MCI-CN contrasts, their ANOVA sample F statistic and *p* value, repeated measures permuted F statistic and *p* value, permutation estimated *post hoc* pair-wise *t* test *p* value, pair-wise Cohen's *d*, and group averages.

Copyright © 2017. NuroSci, LLC.

6. Supplementary Information Table 6 (Right Hemisphere Source ROI MCI-CN Contrast ANOVA Results)

Excel table containing right 12 significant MCI-CN contrasts, their ANOVA sample F statistic and *p* value, repeated measures permuted F statistic and *p* value, permutation estimated *post hoc* pair-wise *t* test *p* value, pair-wise Cohen's *d*, and group averages.

SUBMISSION DRAFT – FOR REVIEW ONLY.
Copyright © 2017. NuroSci, LLC.

References

Albert, M. S. The diagnosis of mild cognitive impairment due to Alzheimer's disease: Recommendations from the National Institute on Aging-Alzheimer's Association workgroups on diagnostic guidelines for Alzheimer's disease. *Alzheimer's & Dementia.* **7**, 270-279 (2011).

Benjamini, Y. and Hochberg, Y. Controlling the false discovery rate: A practical and powerful approach to multiple testing. *J. Roy. Statist. Soc. Ser. B* **57**, 289-300 (1995).

Brier, M. R., et al. Loss of intranetwork and internetwork resting state functional connections with Alzheimer's disease progression. *J Neurosci.* **32**, 8890-8899 (2012).

Buckner, R. L., et al. Molecular, structural, and functional characterization of Alzheimer's disease: evidence for a relationship between default activity, amyloid, and memory. *J. Neurosci.* **25**, 7709-17 (2005).

Cai, S., et al. Changes in thalamic connectivity in the early and late stages of amnestic mild cognitive impairment: a resting-state functional magnetic resonance study from ADNI. *PLoS ONE* 10(2): e0115573 (2015).

Cox, R. W. AFNI: software for analysis and visualization of functional magnetic resonance neuroimages. *Comp Biomed Res.* **29**, 1762-173 (1996).

Dale, A.M., Fischl, B., and Sereno, M.I. Cortical surface-based analysis. I. Segmentation and surface reconstruction. *Neuroimage* **9**, 179-194 (1999).

Davatzikos, C., et al. Longitudinal progression of Alzheimer's-like patterns of atrophy in normal older adults: the SPARE-AD index. *Brain*. **132**, 2026-2036 (2009).

Copyright © 2017. NuroSci, LLC.

Dillen, K. N. H., et al. Functional disintegration of the default mode network in prodromal Alzheimer's disease. *J Alzheimer's Disease*. **59**:169–187. (2017).

Efron, B. Large-scale inference: Empirical Bayes methods for estimation, testing and prediction. IMS Monographs. Cambridge: Cambridge University Press (2010).

Eklund, A., Nichols, T. E., and Knutsson, H. Cluster failure: Why fMRI inferences for spatial extent have inflated false-positive rates. *Proc. Natl. Acad. Sci. USA.* **113**, 7900-7905 (2016).

Fan, Y., et al. m Spatial patterns of brain atrophy in MCI patients, identified via high-dimensional pattern classification, predict subsequent cognitive decline. *Neuroimage*. **39**, 1731-1743 (2008).

Greicius, M. D., Srivastava, G., Reiss, A. L., and Menon, V. Default-mode network activity distinguishes Alzheimer's disease from healthy aging: evidence from functional MRI. *Proc. Natl. Acad. Sci. USA* **101**, 4637-4642 (2004).

Jack, C. R., et al. The Alzheimer's disease neuroimaging initiative (ADNI): MRI methods. *J. Magn. Reson Imaging.* **27**, 685–691 (2008).

Jack, C. R. Introduction to the recommendations from the National Institute on Aging-Alzheimer's Association workgroups on diagnostic guidelines for Alzheimer's disease. *Alzheimer's & Dementia.* **7**, 257-262 (2011).

Jack, C. M. Alliance for aging research AD biomarkers group: structural MRI. *Neurobiol. Aging*. **32**, S48-S57 (2011).

Copyright © 2017. NuroSci, LLC.

Jack, C. R., et al. Update on hypothetical model of Alzheimer's disease biomarkers. *Lancet Neurol.* **12**, 207-216 (2013).

Jones, D.T., et al. Age-related changes in the default mode network are more advanced in Alzheimer disease. *Neurology*. **77**, 1524-1531 (2011).

Jones, D.T., et al. Non-stationarity in the resting brain's modular architecture. *PLoS ONE* 7(6) e39731 (2012).

Klunk, W. E. Imaging brain amyloid in Alzheimer's disease with Pittsburgh Compound-B. *Ann. Neurol.* **55**, 306-19 (2004).

McKhann, G. M. The diagnosis of dementia due to Alzheimer's disease: recommendations from the National Institute on Aging-Alzheimer's Association workgroups on diagnostic guidelines for Alzheimer's disease. *Alzheimer's & Dementia.* **7**, 263-269 (2011).

Misra, C., Fan, Y. and Davatzikos, C. Baseline and longitudinal patterns of brain atrophy in MCI patients, and their use in prediction of short-term conversion to AD: results from ADNI. *Neuroimage*. **44**, 1415-1422 (2009).

Nichols, T. E. and Holmes, A. P. Nonparametric permutation tests for functional neuroimaging: A primer with examples. *Human Brain Mapp.* **15**, 1-25 (2002).

Sorensen, L., et al. Early detection of Alzheimer's disease using MRI hippocampal texture. *Hum. Brain Mapp.* 37, 1148-1161 (2016).

Sorg, et al. Selective changes of resting-state networks in individuals at risk for Alzheimer's disease. *Proc. Natl. Acad. Sci. USA.* **104**, 18760-18765 (2007).

Copyright © 2017. NuroSci, LLC.

Sperling, R. A. Toward defining the preclinical stages of Alzheimer's disease: Recommendations from the National Institute on Aging-Alzheimer's Association workgroups on diagnostic guidelines for Alzheimer's disease. *Alzheimer's & Dementia.* **7**, 280-292 (2011).

Vinters, H. V. Emerging concepts in Alzheimer's disease. *Annu. Rev. Pathol. Mech. Dis.* **10**, 291–319 (2015).

Ward, A. M., et al. The parahippocampal gyrus links the default-mode cortical network with the medial temporal lobe memory system. Hum Brain Mapp. **35**:1061–1073. (2014).

Weiner, M.W., et al. Impact of the Alzheimer's disease neuroimaging initiative, 2004 to 2014. *Alzheimer's Dement.* **11**, 865-884 (2015).

Wolk, D. A., et al. Medial temporal lobe subregional morphometry using high resolution MRI in Alzheimer's disease. *Neurobiol. Aging*. 49:204-213 (2017).

Woo, C-W., Chang, L. J., Lindquist and Wager, T. D. Building better biomarkers: brain models in translational neuroimaging. *Nat Neurosci.* **20**, 365-376 (2017).

Zhou, J., et al. Divergent network connectivity changes in behavioral variant frontotemporal dementia and Alzheimer's disease. *Brain*. **133**, 1352-1367 (2010).

Copyright © 2017. NuroSci, LLC.

Figures

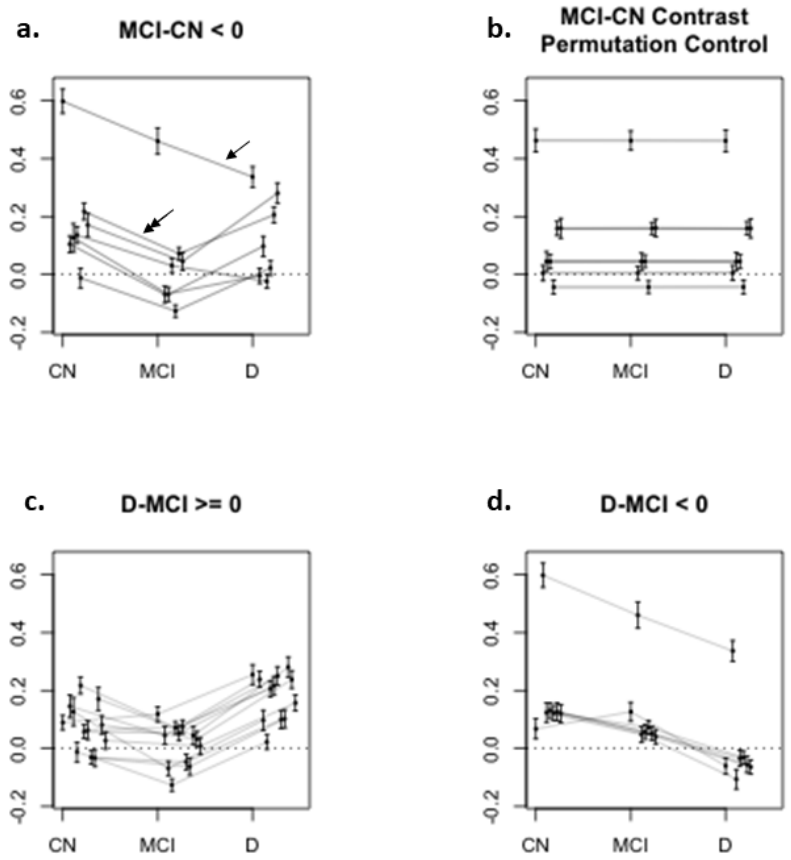

Figure 1. Left hemisphere ROI functional connectivity changes with Alzheimer's disease progression. A plotted point in each panel is the group average Fisher Z-transformed, Pearson pairwise correlation coefficient and standard error of the mean (y axis) for an ROI pair consisting of a left hemisphere anatomically bootstrapped ROI in left MTL, and an ROI which could be either in the left or right hemisphere. Plotted lines connect the same functional pair across diagnostic states (x axis). One-way, three-factor ANOVA tests for source-target ROI pairs (with FDR correction, q=0.05, for multiple hypotheses, N = 9,591) yielded 21 significant ROI pairs. **(a)** Seven of 21 ANOVA significant ROI pairs were significant and negative for the MCI-CN contrast *post hoc* pairwise t test (FDR correction, q=0.05, for multiple hypotheses, N=21). In six

Copyright © 2017. NuroSci, LLC.

of seven cases, the paired ROI was in the right hemisphere. The single-headed arrow points to an ROI pair whose spatial correlation maps are shown in Figure 2. The double-headed arrow points to an ROI pair whose spatial correlation maps are shown in Supplementary Data Figure 1. There were no significant positive MCI-CN contrasts. **(b)** Repeated measures ANOVA by permuted clinical labels (N=5000 trials) shows no effect for any of the seven ROI pairs shown in **(a)**. **(c)** Twelve (12) of 21 ANOVA significant ROI pairs were significant and *positive* for the D-MCI contrast *post hoc* pairwise *t* test. **(d)** Seven (7) of 21 ANOVA significant ROI pairs were significant and *negative* for the D-MCI contrast *post hoc* pairwise *t* test.

SUBMISSION DRAFT – FOR REVIEW ONLY.
Copyright © 2017. NuroSci, LLC.

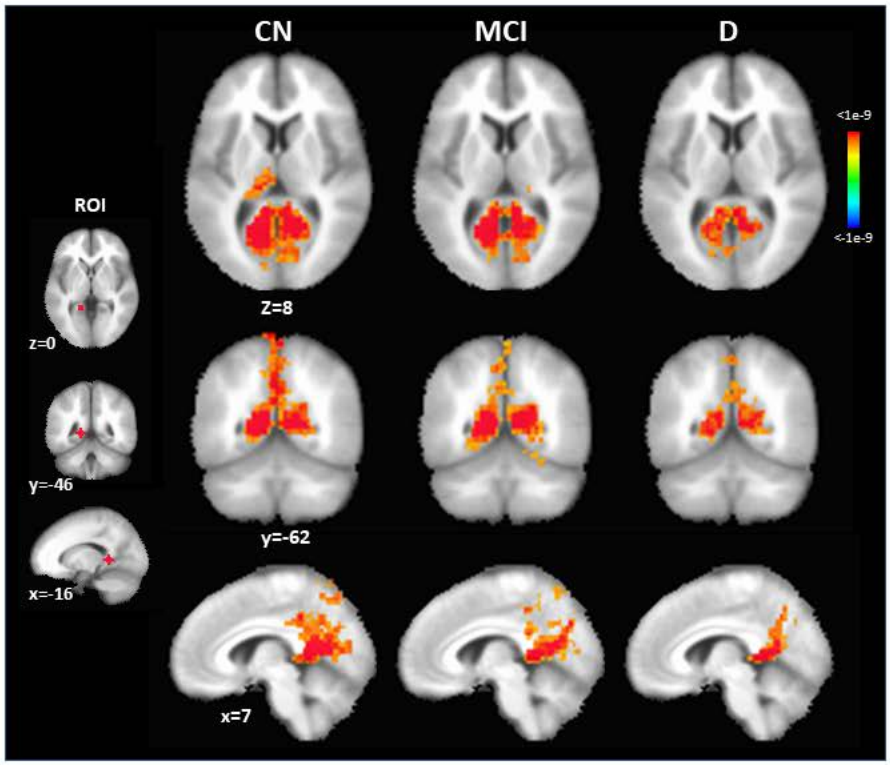

Figure 2. Volumetric representation of functional connectivity changes corresponding to an ROI pair with significant MCI-CN contrast. (The ROI pair treated in this Figure is the one highlighted by small single-headed arrow in Figure 1(a)). Shown in the left-most column is one ROI mask centered at (-14, -44, 4) in MNI coordinates in the AFNI MNI152 atlas in a region containing left parahippocampal gyrus, Brodmann Area 30, and posterior cingulate cortex. Voxel-wise Fisher z-transformed Pearson correlation coefficient maps for CN (*2nd column*), MCI (*3rd column*), and D (*4th column*) clinical groups with axial (*top row*), coronal (*middle*) and sagittal (*bottom*) are shown for fixed position (7, -62, 8) (right cuneus and Brodmann Area 30). For this

Copyright © 2017. NuroSci, LLC.

cross-hemispheric ROI pair, in addition to a significant negative MCI-CN contrast, there was a significant negative D-MCI contrast. The spatial correlation maps were generated by cluster analysis with cluster detection threshold, $P_{CDT} < 1.0 \times 10^{-6}$, minimum cluster size, $N_C = 200$; and color scale maximum threshold, $P_{CMT} < 1.0 \times 10^{-9}$. Display of clusters outside of the immediate region of the ROIs is suppressed. Statistically significant results were tested and confirmed only for the 6 mm ROI pair. Thus, the volumetric data in the region around the ROI indicates trend only.

SUBMISSION DRAFT – FOR REVIEW ONLY.
Copyright © 2017. NuroSci, LLC.

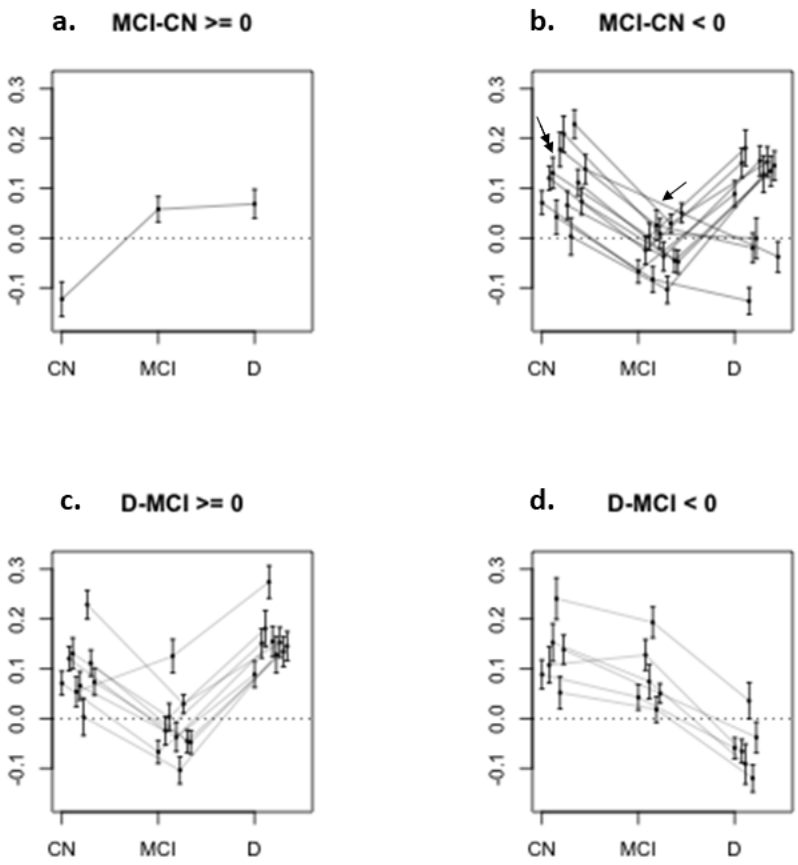

Figure 3. Right hemisphere ROI functional connectivity changes with Alzheimer's disease progression. One-way, three-factor ANOVA tests for 17,766 functional pairs (with FDR correction for multiple hypotheses) yielded 19 significant ROI pairs. **(a)** One of 19 ANOVA significant ROI pairs was significant and *positive* for the MCI-CN contrast *post hoc* pairwise *t* test. **(b)** 12 of 19 ANOVA significant ROI pairs were significant and *negative* for the MCI-CN contrast *post hoc* pairwise *t* test. **(c)** Nine of 19 ANOVA significant ROI pairs were significant and *positive* for the D-MCI contrast *post hoc* pairwise *t* test. **(d)** Six of 19 ANOVA significant ROI pairs were significant and *negative* for the D-MCI contrast *post hoc* pairwise *t* test. The

Copyright © 2017. NuroSci, LLC.

single-headed arrow points to an ROI pair with monotonic loss of functional connectivity with Alzheimer's disease progression. Corresponding volumetric correlation maps are shown in Figure 4. Supplementary Figure 3 illustrates 3D volumetric correlation maps for an ROI pair whose functional connectivity changes are non-monotonic (identified by the double-headed arrow in Panel (b)).

SUBMISSION DRAFT – FOR REVIEW ONLY.
Copyright © 2017. NuroSci, LLC.

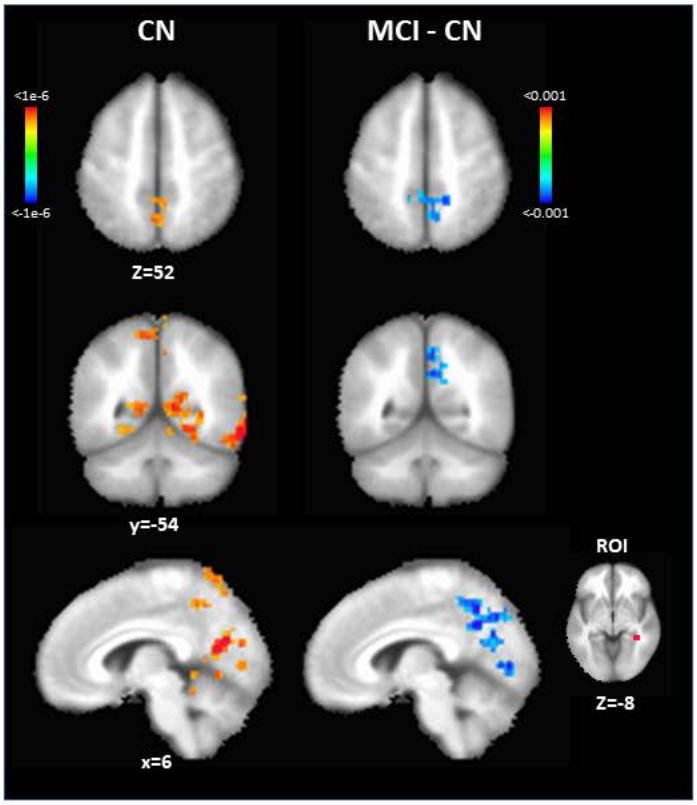

Figure 4. Volumetric correlates of functional connectivity changes corresponding to a right intrahemispheric ROI pair with significant MCI-CN contrast. (The ROI pair treated in this Figure is the one highlighted by small single-headed arrow in Figure 3(a)). Shown on the bottom right is the position of a portion of the ROI mask centered at (34, -36, -8) in the region of right parahippocampal gyrus and hippocampus (CA). Voxel-wise Fisher z-transformed Pearson correlation coefficient maps for CN (left column) with axial (*top row*), coronal (*middle*) and sagittal (*bottom*) are shown for ROI at fixed position (6, -54, 52) (neighboring structures include precuneus and superior parietal lobe). For the MCI-CN contrast, voxel-wise *post hoc* pair-wise *t*

Copyright © 2017. NuroSci, LLC.

statistic maps are shown (*right column*). For this intrahemispheric ROI pair, in addition to a significant negative MCI-CN contrast, there was a significant negative D-MCI contrast. For the CN maps, cluster analysis was with $P_{CDT} < 5.0 \times 10^{-4}$, $N_C = 100$; and $P_{CMT} < 1.0 \times 10^{-6}$. For the MCI-CN maps, cluster analysis was with $P_{CDT} < 5.0 \times 10^{-3}$, $N_C = 20$; and $P_{CMT} < 1.0 \times 10^{-3}$. Display of clusters outside of the immediate region of the ROI is suppressed.

Copyright © 2017. NuroSci, LLC.

Supplementary Figures

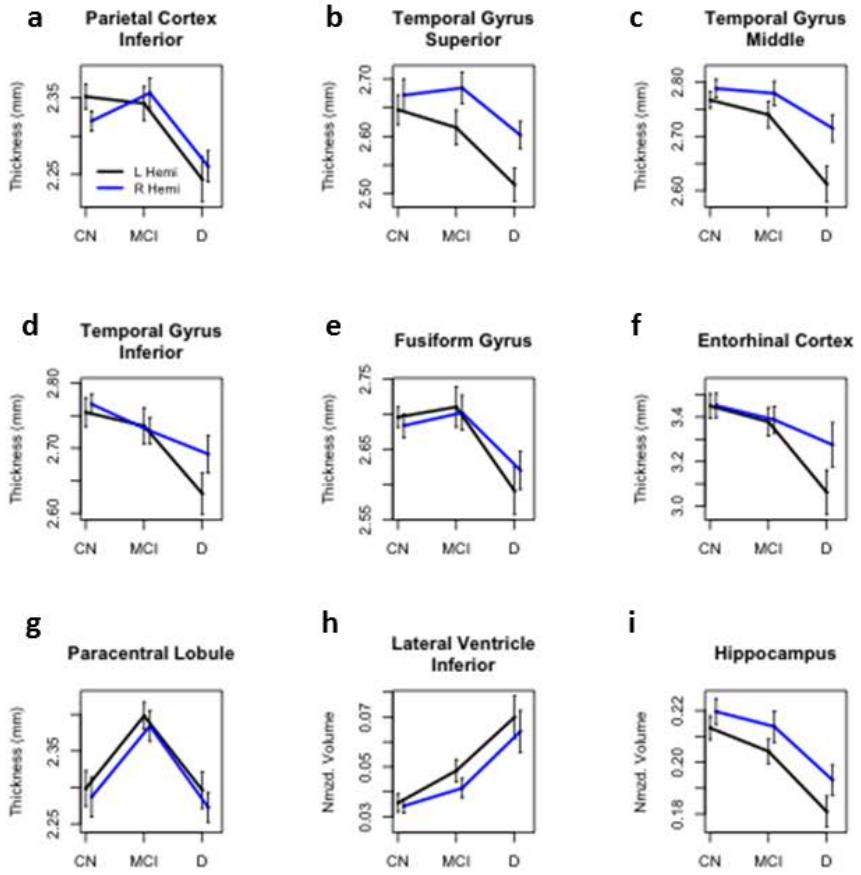

Supplementary Figure 1. Representative progression of cortical thinning and subcortical structure volume. ***(a-g)*****:** Representative left and right hemisphere CN, MCI and D diagnosis group average and standard error of FreeSurfer 6.0 estimates of labelled regional cortical layer thickness where one or both hemispheres were significant in a one-way, three-factor (CN, MCI, D), ANOVA, FDR-corrected (q=0.1, 68 tests) procedure. For significant ANOVA tests (23 of 68), FDR corrected, *post hoc* pairwise t tests were computed for the three contrasts MCI-CN, D-CN, and D-MCI. There were two significant MCI-CN contrasts (left and right paracentral, panel (g)); fifteen significant D-CN contrasts; and twenty-one significant D-MCI contrasts. ***(h-i)*****:**

Copyright © 2017. NuroSci, LLC.

Representative left and right hemisphere CN, MCI and D clinical group average and standard error of FreeSurfer 6.0 estimates of labelled subcortical structure volume where one or both hemispheres were significant in a one-way, three-factor (CN, MCI, D), ANOVA, FDR-corrected (q=0.1, 16 tests). For significant ANOVA tests (8 of 16), FDR corrected, post hoc pairwise t tests were computed for the three contrasts MCI-CN, D-CN, and D-MCI. There were eight significant D-CN contrasts and six significant D-MCI contrasts. There were no significant MCI-CN contrasts.

Copyright © 2017. NuroSci, LLC.

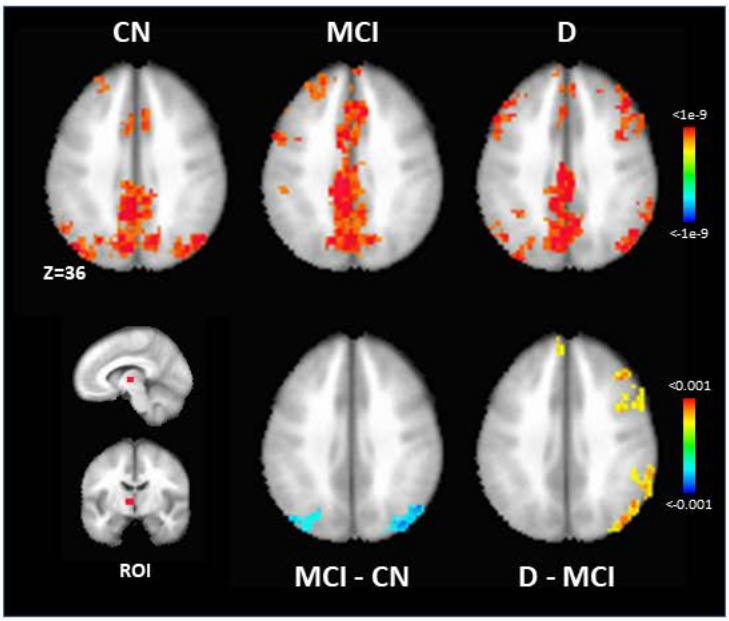

Supplementary Figure 2. Volumetric correlates of functional connectivity changes corresponding to a left intrahemispheric ROI pair with significant MCI-CN contrast. (The pair treated in this Figure is the one highlighted by small double-headed arrow in Figure 1(a)). Shown in the bottom left is the source ROI mask centered at (-6, -12, 4) in MNI coordinates in the AFNI MNI152 atlas as left thalamus (medial dorsal nucleus; ventral lateral nucleus). Voxel-wise Fisher z-transformed Pearson correlation coefficient axial maps for CN (*top row, left*), MCI (*top row, middle*), and D (*top row, right*) clinical groups with axial (*top row*), coronal (*middle*) and

Copyright © 2017. NuroSci, LLC.

sagittal (*bottom*) are shown for fixed position (48, -69, 36) (right angular gyrus; Brodmann Area 39; inferior parietal cortex). Shown in the second row are the spatial maps of *post hoc* pair-wise *t* test statistics for MCI-CN and D-CN. For this ROI pair, the significant negative MCI-CN contrast is followed by a significant positive D-MCI contrast. The spatial correlation maps were generated by cluster analysis with $P_{CDT} < 5.0 \times 10^{-5}$, $N_C = 100$; and $P_{CMT} < 1.0 \times 10^{-8}$. The spatial *t* statistic maps were generated by cluster analysis with $P_{CDT} < 0.05$, $N_C = 100$; and, $P_{CMT} < 0.001$. Display of clusters outside of the immediate region of the target ROI is suppressed.

SUBMISSION DRAFT – FOR REVIEW ONLY.
Copyright © 2017. NuroSci, LLC.

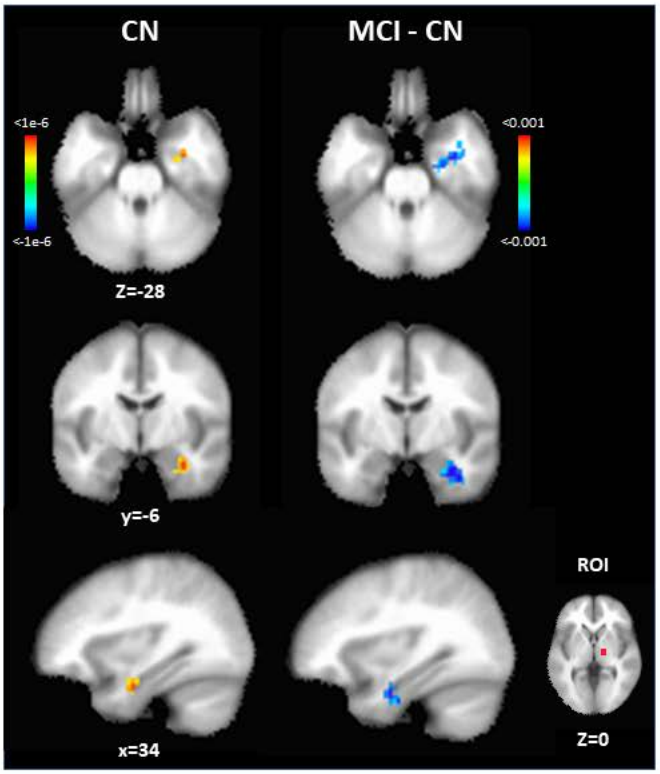

Supplementary Figure 3. Volumetric correlates of functional connectivity changes corresponding to a right intrahemispheric ROI pair with significant MCI-CN contrast. (The source-target pair treated in this Figure is the one highlighted by small double-headed arrow in Figure 3(a)). Shown on the bottom right is the position of a portion of the ROI mask centered at (12, -14, 0) in the region of right thalamus (ventral lateral nucleus). Voxel-wise Fisher z-transformed Pearson correlation coefficient maps for CN (left column) with axial (*top row*), coronal (*middle*) and sagittal (*bottom*) are shown for target ROI at fixed position (34, -6, -28) (neighboring structures include hippocampus and perirhinal cortex). For the MCI-CN contrast,

Copyright © 2017. NuroSci, LLC.

voxel-wise *post hoc* pair-wise *t* statistic maps are shown (*right column*). For this intrahemispheric source-target ROI pair, in addition to a significant negative MCI-CN contrast, there was a significant positive D-MCI contrast (not shown). For the CN maps, cluster analysis was with $P_{CDT} < 5.0 \times 10^{-4}$, $N_C = 100$; and $P_{CMT} < 1.0 \times 10^{-6}$. For the MCI-CN maps, cluster analysis was with $P_{CDT} < 5.0 \times 10^{-3}$, $N_C = 20$; and $P_{CMT} < 1.0 \times 10^{-3}$. Display of clusters outside of the immediate region of the target ROI is suppressed.

SUBMISSION DRAFT – FOR REVIEW ONLY.
Copyright © 2017. NuroSci, LLC.

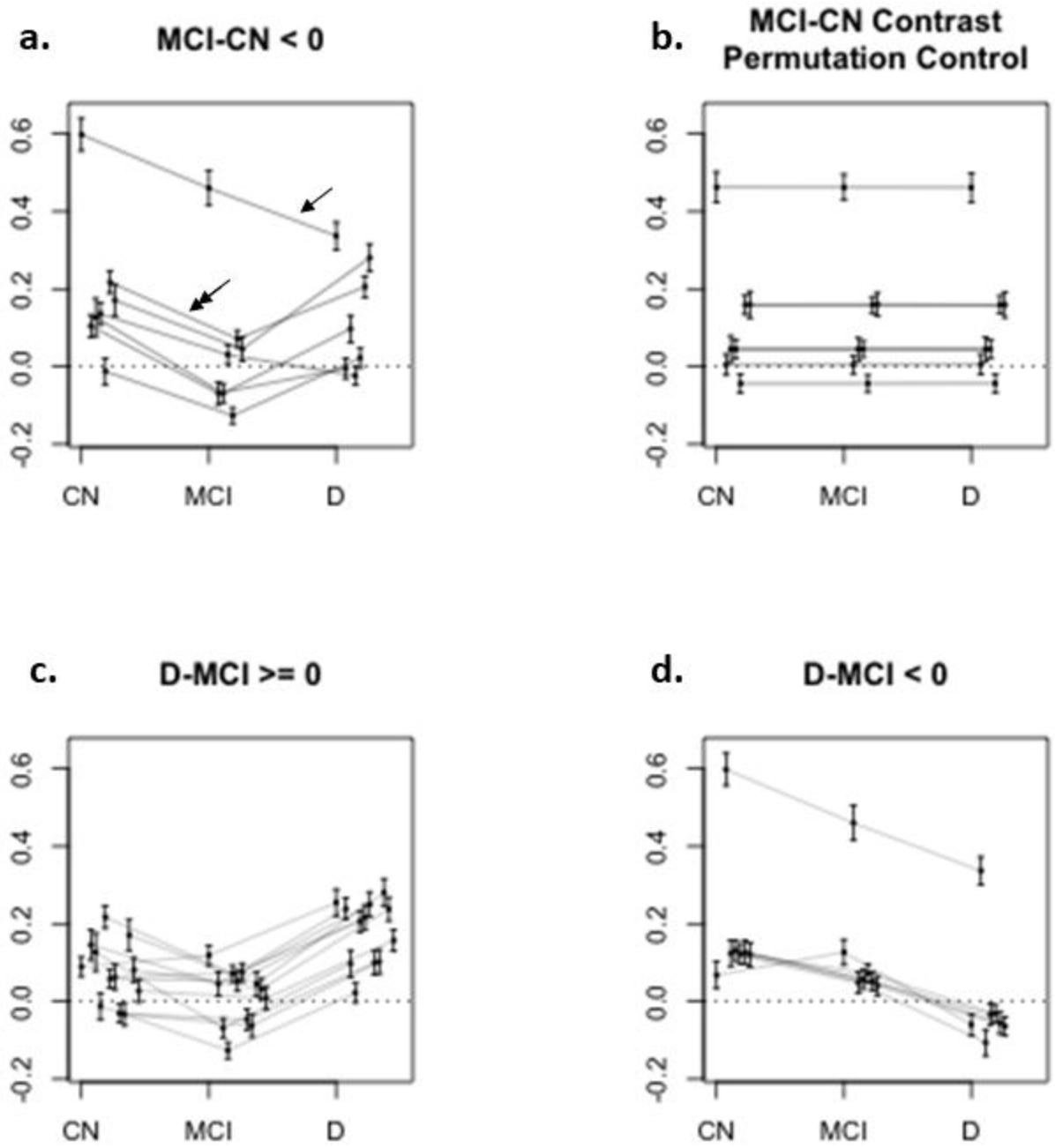
a.
MCI-CN < 0
b.
MCI-CN Contrast
Permutation Control
c.
D-MCI >= 0
d.
D-MCI < 0
0.6
0.4
0.2
0.0
-0.2
CN
MCI
D

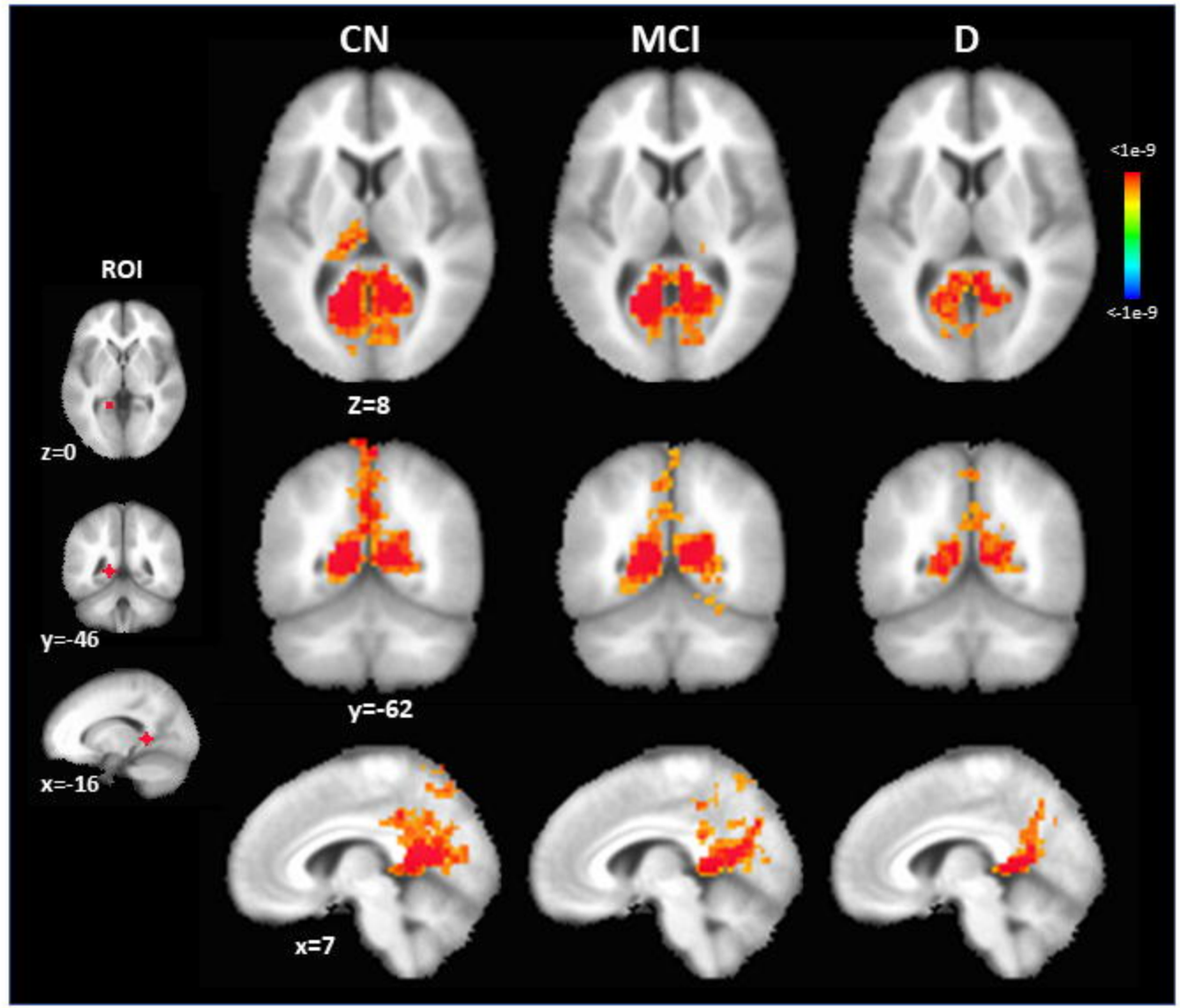
CN
MCI
D
ROI
z=0
y=-46
x=-16
Z=8
y=-62
x=7
<1e-9
<-1e-9

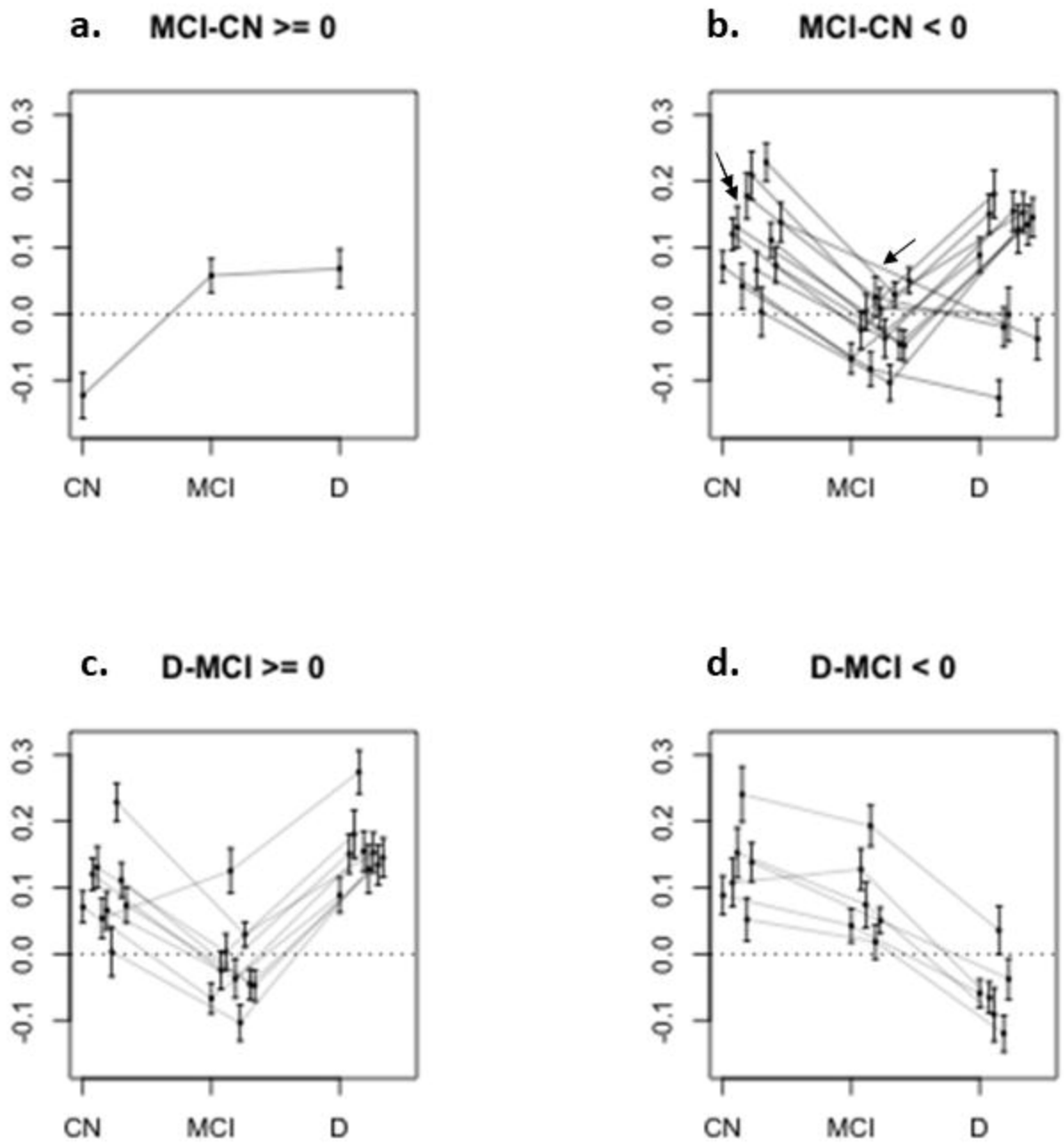
a. MCI-CN >= 0
b. MCI-CN < 0
c. D-MCI >= 0
d. D-MCI < 0
-0.1
0.0
0.1
0.2
0.3
CN
MCI
D

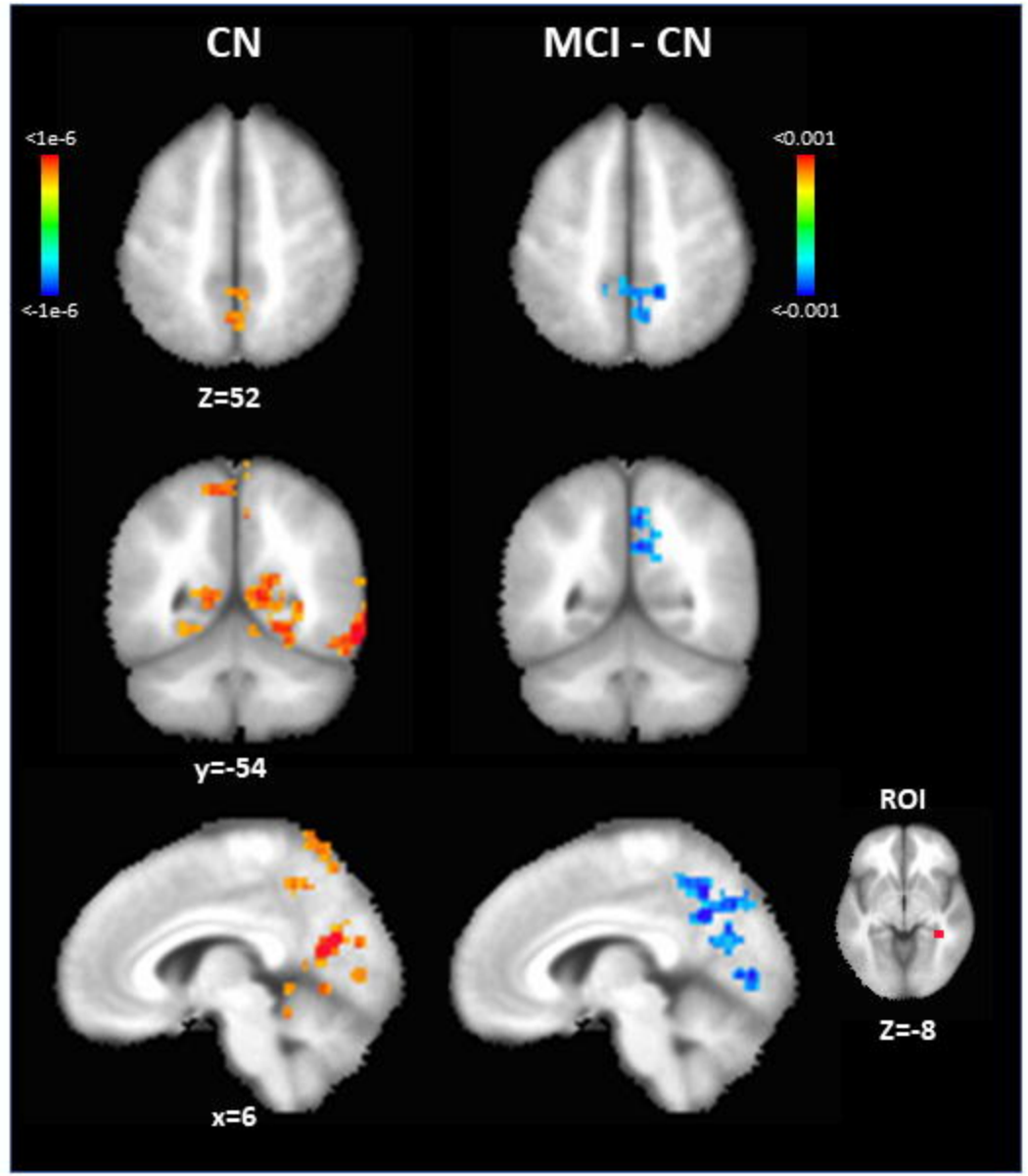
CN
MCI - CN
<1e-6
<-1e-6
<0.001
<-0.001
Z=52
y=-54
ROI
Z=-8
x=6

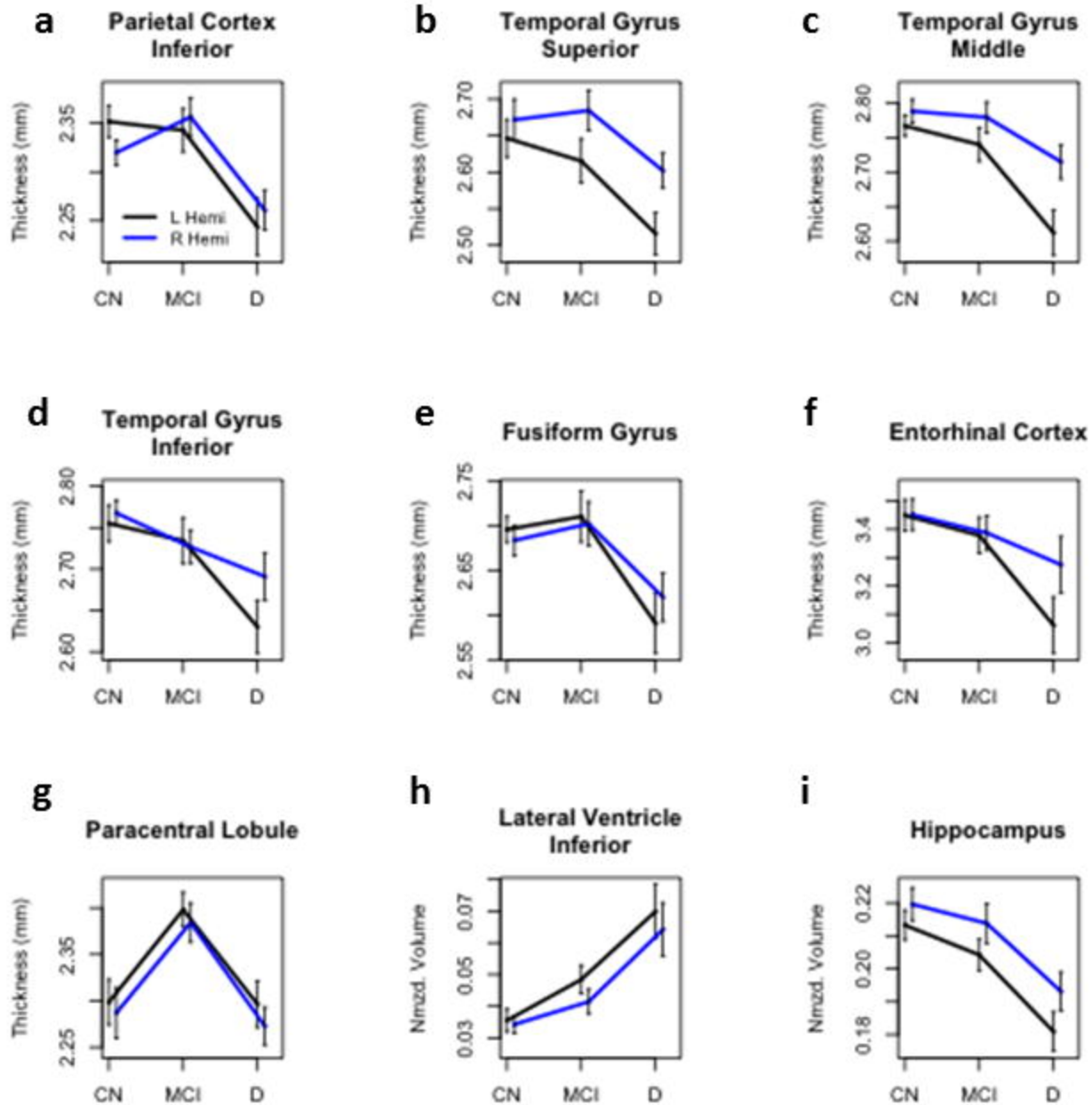
a
Parietal Cortex Inferior
Thickness (mm)
2.25
2.35
L Hemi
R Hemi
CN
MCI
D
b
Temporal Gyrus Superior
Thickness (mm)
2.50
2.60
2.70
CN
MCI
D
c
Temporal Gyrus Middle
Thickness (mm)
2.60
2.70
2.80
CN
MCI
D
d
Temporal Gyrus Inferior
Thickness (mm)
2.60
2.70
2.80
CN
MCI
D
e
Fusiform Gyrus
Thickness (mm)
2.55
2.65
2.75
CN
MCI
D
f
Entorhinal Cortex
Thickness (mm)
3.0
3.2
3.4
CN
MCI
D
g
Paracentral Lobule
Thickness (mm)
2.25
2.35
CN
MCI
D
h
Lateral Ventricle Inferior
Nmzd. Volume
0.03
0.05
0.07
CN
MCI
D
i
Hippocampus
Nmzd. Volume
0.18
0.20
0.22
CN
MCI
D

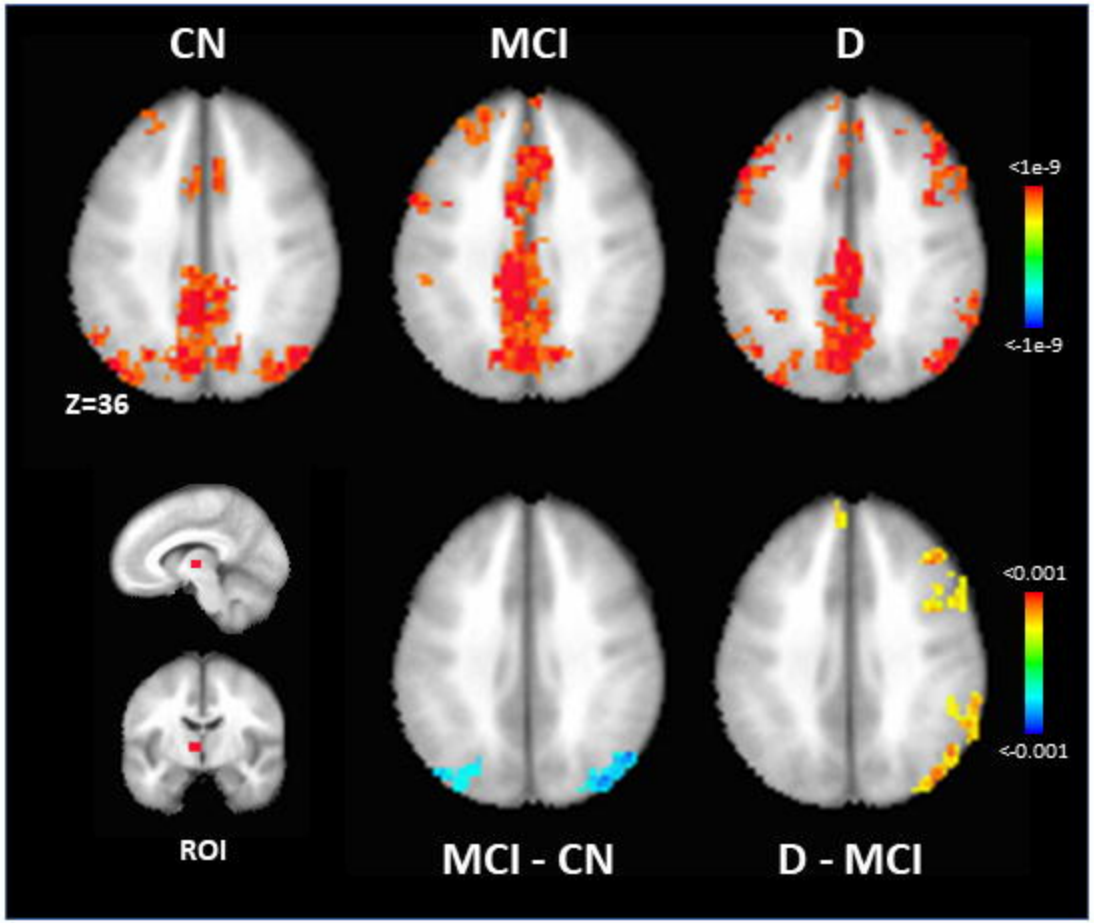
CN
MCI
D
<1e-9
<-1e-9
Z=36
<0.001
<-0.001
ROI
MCI - CN
D - MCI

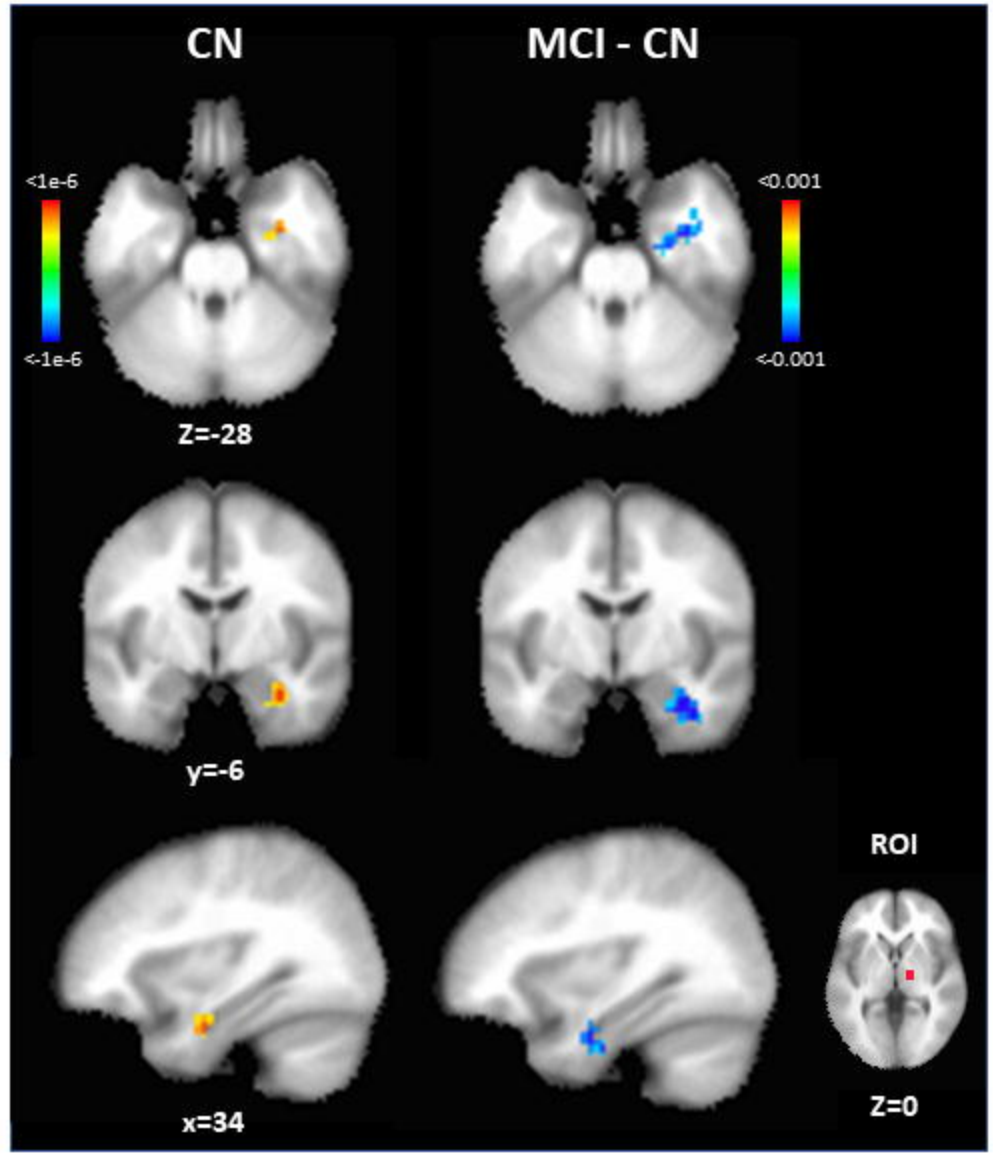
CN
MCI - CN
<1e-6
<-1e-6
<0.001
<-0.001
Z=-28
y=-6
x=34
ROI
Z=0